CMS Physics Analysis Summary

Contact: cms-pag-conveners-higgs@cern.ch 2016/02/02

Search for the exotic decay of the Higgs boson to two light pseudoscalar bosons with two taus and two muons in the final state at $\sqrt{s} = 8$ TeV

The CMS Collaboration

Abstract

A search for the exotic decay of the Higgs boson to a pair of light pseudoscalar a bosons is performed in the final state with two muons and two taus. The motivation lies in models beyond the standard model, such as two-Higgs-doublet models extended with a complex singlet (2HDM+S). The results are based on an integrated luminosity of 19.7 fb^{-1}, accumulated by the CMS experiment at LHC in 2012 at 8 TeV center-of-mass energy. Masses of the pseudoscalar boson between 20 and 62.5 GeV are probed, and upper limits between 4 and 15% are set on the branching fraction of the Higgs boson to two light pseudoscalar bosons, under the hypothesis that the pseudoscalar a does not decay to quarks.

1 Introduction

The discovery of a standard-model-like Higgs scalar (h) has been a triumph of the standard model (SM) [1, 2]. Up to now, all its properties have been measured to be compatible with the SM Higgs boson. Nevertheless, current results by ATLAS and CMS still allow for exotic h decays [3–5].

Two-Higgs-doublet models (2HDM) introduce two Higgs doublets, which, after symmetry breaking, lead to five physical states. One of the free parameters in 2HDM is $\tan\beta$, the ratio between the vacuum expectation values of the two doublets. The lightest scalar of 2HDM can be compatible with the SM-like properties of the discovered boson in the decoupling limit, where other scalars all have large masses. A complex $SU(2)_L$ singlet field S can be added to 2HDM, with a small mixing with the doublets; such a model is called 2HDM+S. This leads to two additional singlet states, a CP-odd scalar a and a CP-even s, which inherit a mixture of the Higgs doublets fermion interactions. In such a model, the branching fraction of the h boson to a pair of a or s bosons can be sizeable, and a wide variety of exotic h decays is allowed [6].

Motivations for the existence of exotic decays of the h boson to non-SM particles are various [7]. First, the SM Higgs boson has an extremely narrow width ($\Gamma_h \simeq 4.07$ MeV) compared to its mass, because of the suppression of tree-level Yukawa couplings. The coupling, even small, to a non-SM light state could open non negligible decay modes. Second, the scalar sector could be a portal to new physics, which allows SM matter to interact with a hidden-sector matter. The so-called Higgs portal [8] allows the hidden-sector matter not to be charged under SM forces. And finally, exotic decays are a relatively simple extension of the SM, and are still allowed after all the measurements made during LHC Run 1.

The branching fractions of the pseudoscalar a to SM particles depend on the model. In 2HDM+S type-1, the couplings of the pseudoscalar to fermions are SM-like; whereas in 2HDM+S type-2 (next-to-minimal-supersymmetric-SM-like), they are suppressed for down-type fermions for $\tan\beta < 1$ (and increased for $\tan\beta > 1$). In 2HDM+S type-3, the decays to leptons are enhanced with respect to the decays to quarks for $\tan\beta > 1$, and in 2HDM+S type-4, the decays to up-type quarks and leptons are enhanced for $\tan\beta < 1$.

An upper limit on the branching fraction of the h boson to BSM particles can be set from direct measurements on its properties and, as of today, this upper limit leaves a large room for exotic decays. CMS indeed measured $\mathcal{B}(h \to BSM) < 32\%$ at 95% CL, using all data collected during LHC Run 1 [3].

The $h \to aa \to \mu\mu\tau\tau$ process can be studied to uncover an eventually exotic scalar sector. This channel has two easily detectable muons in the final state, with an excellent mass resolution. In addition, in comparison to final states with b quarks, the decay of the other a boson to two taus leads to a good mass resolution for the second pair and to an efficient background rejection. Finally the branching fraction of the a boson to tau leptons is much larger than its branching fraction to muons, leading to a larger number of expected events for $h \to aa \to \mu\mu\tau\tau$ than $h \to aa \to \mu\mu\mu\mu$, when kinematically allowed. The largest $\mathcal{B}(aa \to \mu\mu\tau\tau)$ is obtained at large $\tan\beta$ in 2HDM+S type-3, and can be as large as a few permille. The results are based on an integrated luminosity of 19.7 fb^{-1}, accumulated by the CMS experiment at LHC in 2012 at 8 TeV center-of-mass energy, and target pseudoscalar masses between 20 GeV and half of the h boson mass, 62.5 GeV.

Other analyses have been looking for exotic $h \to aa$ decays in data collected during the first run of the LHC, without finding any hint for the existence of new physics beyond the SM. ATLAS has performed a search for $h \to aa \to \mu\mu\tau\tau$ for pseudoscalar masses m_a such that $2m_\tau < m_a <$

50 GeV [9], using special techniques to reconstruct boosted tau leptons. The CMS searches for exotic $h \to aa$ decays include $h \to aa \to \mu\mu\mu\mu$ for $2m_\mu < m_a < 2m_\tau$ [10], and $h \to aa \to \tau\tau\tau\tau$ for $2m_\tau < m_a < 15$ GeV [11, 12].

2 CMS detector and samples

The central feature of the CMS apparatus is a superconducting solenoid of 6 m internal diameter, providing a magnetic field of 3.8 T. Within the superconducting solenoid volume are a silicon pixel and strip tracker, a lead tungstate crystal electromagnetic calorimeter (ECAL), and a brass and scintillator hadron calorimeter (HCAL), each composed of a barrel and two endcap sections. Muons are detected in gas-ionization detectors embedded in the steel flux-return yoke outside the solenoid. Extensive forward calorimetry complements the coverage provided by the barrel and endcap detectors. A more detailed description of the CMS detector, can be found in Ref. [13].

A set of simulated samples is used to produce the mixture of signal and backgrounds. The ZZ diboson samples are generated with MADGRAPH [14]. Signal samples are produced for pseudoscalar boson masses between 20 and 60 GeV, using PYTHIA [15]. The tau lepton decays are simulated with TAUOLA [16]. Minimum bias events generated by PYTHIA are added to all generated Monte Carlo (MC) samples. Simulated events are reweighted in order to match the number of pile-up interactions expected. All generated events are passed through the full GEANT [17] based simulation of the CMS apparatus and are reconstructed using the same version of the CMS event reconstruction software as the data.

3 Object reconstruction and event selection

The events are selected with two muons and two tau leptons. Five different final states are studied, depending on whether the tau leptons decay to electrons (τ_e), to muons (τ_μ) or hadronically (τ_h): $\mu\mu\tau_e\tau_e$, $\mu\mu\tau_e\tau_\mu$, $\mu\mu\tau_e\tau_h$, $\mu\mu\tau_\mu\tau_h$ and $\mu\mu\tau_h\tau_h$. The $\mu\mu\tau_\mu\tau_\mu$ final state is not considered in this analysis because of its low sensitivity and of the difficulty in matching the four muons in two correct pairs.

The event reconstruction relies on the particle flow (PF) algorithm, which combines information from different subdetectors to reconstruct individual particles [18, 19]. Muons are reconstructed by matching hits in the silicon tracker and in the muon system [20]. Electrons are identified with a multivariate (MVA) method trained to discriminate genuine electrons from quark and gluon jets [21]. Some isolation criteria are applied to electrons and muons; their relative isolation is defined as:

$$I_{\text{rel}} = \left[\sum_{\text{charged}} p_T + \max\left(0, \sum_{\text{neutral}} p_T + \sum_{\gamma} p_T - \frac{1}{2} \sum_{\text{charged,PU}} p_T\right)\right] / p_T \quad (1)$$

where $\Sigma_{\text{charged}} p_T$ is the sum of the transverse energy of charged hadrons, electrons and muons originating from the primary vertex, $\Sigma_{\text{neutral}} p_T$ is the same sum for neutral hadrons and Σ_γ for photons, and $\Sigma_{\text{charged,PU}} p_T$ is the sum of the transverse energy of charged hadrons, electrons and muons originating from other reconstructed vertices. The particles considered to build the isolation are in a cone with a radius $\Delta R = \sqrt{\Delta\eta^2 + \Delta\phi^2} = 0.4$ around the lepton direction. Hadronically decaying taus are identified with the Hadron Plus Strip (HPS) algorithm, which matches tracks and ECAL energy deposits to reconstruct tau candidates in one of the

possible tau decay modes [22, 23]. An MVA-based isolation that takes into account tau lifetime information, is used to reject quark and gluon jets. An MVA-based discriminator to reduce the rate with which electrons are misidentified as hadronically decaying taus and another one to reject muons misidentified as hadronically decaying taus are also applied to τ_h candidates. The discriminator working points depend on the final state and are detailed in the following paragraphs.

Events are triggered with an asymmetric di-muon trigger; two reconstructed muons with $p_T >$ 9/18 GeV and $|\eta| < 2.4$ are required to be present and to fire the trigger path.

To reconstruct the di-muon pair coming promptly from an a boson, two muons with an opposite sign charge, $p_T > 5$ GeV and $|\eta| < 2.4$ are selected. They are required to pass the loose working point of the PF muon identification algorithm, and to have a relative isolation less than 0.4. In the $\mu\mu\tau_e\tau_e$, $\mu\mu\tau_e\tau_h$ and $\mu\mu\tau_h\tau_h$ final states, where they are the only muons, their p_T thresholds are raised to 9/18 GeV to match the trigger requirements.

When there are more than two muons in the final state (in the case of $a \to \tau_\mu\tau_h$ and $a \to \tau_\mu\tau_e$ decays), the highest p_T muon is considered as decaying promptly from a. It is paired with the next highest p_T muon with an opposite sign charge. The other muons are considered as coming from a tau decay. The success rate in reconstructing the correct matching for the signal is around 90%.

The candidates forming the di-tau pair are selected with an opposite sign charge. The selection depends on the final state. In the $\mu\mu\tau_e\tau_e$ final state, two electrons with $p_T > 7$ GeV, $|\eta| <$ 2.5, passing the MVA identification and having a relative isolation less than 0.2, are required in addition to the already selected muons. The contribution from $h \to ZZ \to 2\mu 2e$ events is removed by excluding events with the visible invariant mass of the four leptons in a 30 GeV-wide window around the h boson mass. In the $\mu\mu\tau_e\tau_\mu$ final state, an additional muon with $p_T > 5$ GeV (or $p_T > 9$ GeV if it is responsible for firing the trigger path), $|\eta| < 2.4$, tightly identified and with a relative isolation less than 0.2, as well as an electron with $p_T > 7$ GeV, $|\eta| < 2.5$, identified and with a relative isolation less than 0.4 are required. In the $\tau_e\tau_h$ final state, an electron with $p_T > 7$ GeV, $|\eta| <$2.5, identified and with a relative isolation less than 0.2, and a hadronic tau with $p_T > 15$ GeV, $|\eta| < 2.3$, and passing the loose MVA identification, the loose rejection against electrons and the loose rejection against muons are selected. Similarly, for the $\tau_\mu\tau_h$ decay, a muon with $p_T > 5$ GeV (or $p_T > 9$ GeV if it is responsible for firing the trigger path), $|\eta| < 2.4$, tightly identified and with a relative isolation less than 0.25, and a hadronic tau with $p_T > 15$ GeV, $|\eta| < 2.3$, and passing the loose MVA identification, the very loose working point of the discriminator against electrons and the loose working point of the discriminator against muons are required. Finally, in the $\mu\mu\tau_h\tau_h$ final state, two hadronic taus with $p_T > 15$ GeV, $|\eta| < 2.3$, and passing the medium MVA isolation, the loose rejection against electrons and the loose rejection against muons, are selected in addition to the two muons.

In all final states, the four objects are required to be separated from each other by at least $\Delta R =$ 0.4. The events are vetoed if at least one b-tagged jet, with $p_T > 20$ GeV, $|\eta| < 2.4$ and passing the tight working point of the combined secondary vertex (CSV) algorithm [24], is found. This reduces the contribution from backgrounds with top quarks, including $t\bar{t}$ production among others. In order to prevent a single event from entering different final states, events containing other identified and isolated electrons or muons in addition to the four selected objects are rejected ("lepton veto").

Two additional selection criteria are designed to reduce the contribution of the backgrounds to the signal region, and are applied to all final states. First, the invariant mass of the di-muon

Table 1: Selection criteria in the five final states. The two p_T and η values quoted for the muons in the $\mu\mu\tau_\mu\tau_h$ and $\mu\mu\tau_e\tau_\mu$ final states correspond to the case where the muons are responsible or not for firing the trigger path.

	$\mu\mu\tau_e\tau_e$	$\mu\mu\tau_e\tau_\mu$	$\mu\mu\tau_e\tau_h$	$\mu\mu\tau_\mu\tau_h$	$\mu\mu\tau_h\tau_h$
μ_1	$p_T >$18 GeV, $\lvert\eta\rvert < 2.4$, $I_{rel} < 0.4$, Loose PF ID				
μ_2	$I_{rel} < 0.4$, Loose PF ID, $\lvert\eta\rvert < 2.4$				
	$p_T > 9$ GeV	$p_T > 5/9$ GeV	$p_T > 9$ GeV	$p_T > 5/9$ GeV	$p_T > 9$ GeV
τ_e	$p_T > 7$ GeV, $\lvert\eta\rvert < 2.5$, MVA ID			-	-
	$I_{rel} < 0.4$	$I_{rel} < 0.4$	$I_{rel} < 0.2$		
τ_h	-	-	$p_T > 15$ GeV, $\lvert\eta\rvert < 2.3$, Loose anti-μ		
			Loose iso. Loose anti-e	Loose iso. vLoose anti-e	Medium iso. vLoose anti-e
τ_μ	-	$p_T > 9/5$ GeV $\lvert\eta\rvert < 2.4$ Loose PF ID $I_{rel} < 0.4$	-	$p_T > 9/5$ GeV $\lvert\eta\rvert < 2.4$ Tight PF ID $I_{rel} < 0.25$	-
b–Jet veto	No b–tagged jet in the event.				
Lepton veto	No additional identified and isolated electron or muon.				
$\lvert m_{\mu\mu\tau\tau} - 125\rvert$	< 25 GeV				
$\lvert m_{\mu\mu} - m_{\tau\tau}\rvert / m_{\mu\mu}$	< 0.8				
ΔR **between leptons**	> 0.4				
$\lvert m^{vis}_{\mu\mu ee} - 125\rvert$	> 15 GeV	-			

pair and the di-tau pair, is required to lie close to the h boson mass: $|m_{\mu\mu\tau\tau} - 125| < 25$ GeV. The di-tau mass $m_{\tau\tau}$ is fully reconstructed with a maximum likelihood algorithm taking as input the four-momenta of the visible particles, as well as the missing transverse energy and its resolution [25]. Second, as the di-muon pair and the di-tau pair are expected to have the same mass in signal events, a selection criterium on the absolute mass difference between the lepton pairs, normalized over the di-muon pair, is applied: $|m_{\mu\mu} - m_{\tau\tau}|/m_{\mu\mu} < 0.8$. These two cuts have a signal efficiency larger than 95%.

A summary of the criteria applied to select events in the five final states is shown in Tab. 1.

4 Background estimation

Two types of backgrounds contribute to the final states studied in this analysis: irreducible ZZ diboson production, and reducible processes with at least one jet misidentified as one of the leptons. The reducible background is essentially composed of Z+jets and WZ+jets processes.

The $ZZ \to 4\ell$ contribution is estimated directly from MC, and the process is scaled to its next-to-leading order (NLO) cross section [26]. Because of the low number of events passing the selection in the $\mu\mu\tau_h\tau_h$ final state, the di-muon mass ($m_{\mu\mu}$) distribution of the ZZ background is taken from a selection with a relaxed tau isolation for this final state. This does not modify the overall shape but contributes to making it smoother.

The $m_{\mu\mu}$ shape and the normalization of the reducible backgrounds are determined in two different steps. The normalization is obtained with a data-driven method. The rates with which jets are misidentified as hadronic taus, electrons, or muons are measured in dedicated signal-free control regions. These regions are defined similarly as the signal region, except that the

tau candidates (electrons, muons or hadronically decaying taus) are loosely identified and isolated, and carry a same-sign charge. All misidentification rates are measured as a function of the transverse momentum of the jet closest to the tau candidate, and are fitted using a decreasing exponential plus a constant, for transverse momenta of the closest jet larger than 15 GeV. In the case of electrons and muons with the closest jet having a transverse momentum between 5 and 15 GeV, the misidentification rates are measured in two five-GeV-wide bins. Events passing the full signal selection, except the tau candidate (τ_e, τ_μ or τ_h) identification or isolation, are reweighted as a function of the misidentification rates to obtain an estimate of the contribution of the reducible background to the signal region. Double counting is removed by subtracting the weighted contribution of events with two tau candidates failing the isolation or identification criteria, to weighted events with only one tau candidate failing the isolation or identification criteria.

The $m_{\mu\mu}$ shape of the reducible backgrounds is taken from a signal-free region in collision data, where the two tau candidates carry the same charge. To obtain smoother shape templates, the identification and the isolation applied on the tau candidates are relaxed.

Fig. 1 demonstrates a good agreement between data and predicted backgrounds over the full $m_{\mu\mu}$ mass range, when no selection is applied on the variables $m_{\mu\mu}$, $m_{\mu\mu\tau\tau}$ and $|m_{\mu\mu} - m_{\tau\tau}|/m_{\mu\mu}$.

5 Signal and background modeling

Given the good resolution of the di-muon mass for the muons originating promptly from an a boson, an unbinned shape analysis is performed, using $m_{\mu\mu}$ as observable.

5.1 Signal

The di-muon mass distribution in signal events in final states with two muons is parameterized with a Voigtian function, which is the convolution between a Gaussian and a Lorentzian function, and describes well narrow resonances with experimental resolution effects. In final states with three muons, the Gaussian component is found to be negligible, and the signal shapes are parameterized with Lorentzian functions. A distinct fit is performed in every final state and for every generated a boson mass. In order to interpolate the shape templates to intermediary mass points, the parameters of the fit functions are parameterized as a function of the a boson mass by fitting with a third-degree polynomial the parameters of the Voigtian or Lorentzian functions obtained from the individual fits. A similar technique is used to interpolate the signal normalization to intermediate mass points, starting from the normalization of the generated MC samples. A closure test that consists in removing a signal sample corresponding to a given mass point from the parameterization of the Voigtian and Lorentzian fit parameters as a function of the mass, and comparing the parameterization interpolation to the direct fit to this sample has demonstrated the validity of such a technique.

5.2 Backgrounds

The ZZ irreducible background is parameterized with a Bernstein polynomial with five degrees of freedom. This generic function is shown to describe the MC well. The fifth degree is chosen because it improves significantly the fit quality in the $\mu\mu\tau_e\tau_e$ final state compared to the fourth degree, and because the sixth degree brings only a negligible improvement. The ZZ background being subdominant in most final states, the choice of this function over another one does not introduce a bias in expected limits, and no shape uncertainty is considered for this background. The fits performed in all five final states are shown in Fig. 2.

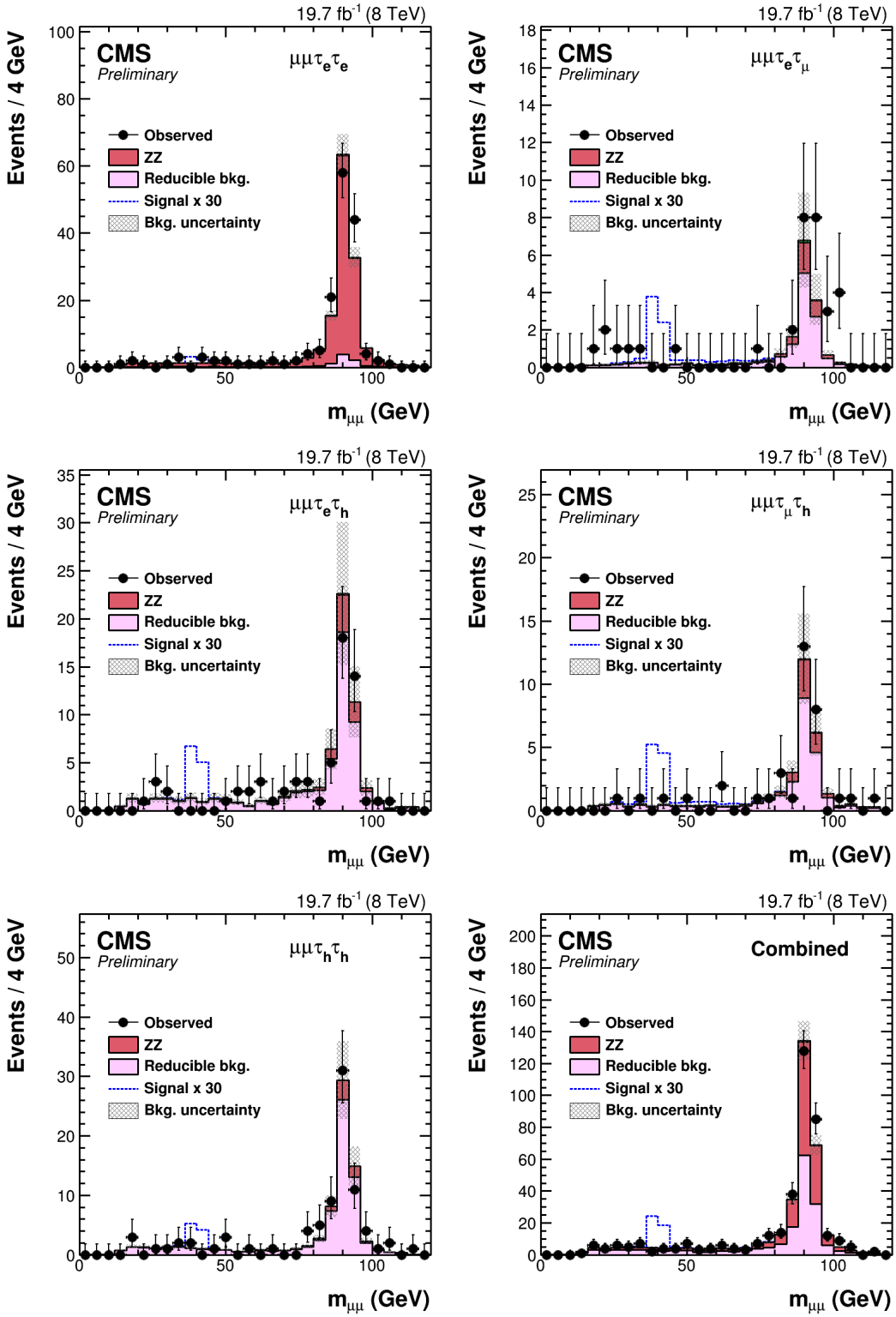

Figure 1: Data, predicted SM backgrounds, and signal ($m_a = 40$ GeV) di-muon mass distributions in the $\mu\mu\tau_e\tau_e$ (top left), $\mu\mu\tau_e\tau_\mu$ (top right), $\mu\mu\tau_e\tau_h$ (center left), $\mu\mu\tau_\mu\tau_h$ (center right), and $\mu\mu\tau_h\tau_h$ (bottom left) final states, and their combination (bottom right). The cuts on the variables $m_{\mu\mu}$, $m_{\mu\mu\tau\tau}$ and $|m_{\mu\mu} - m_{\tau\tau}|/m_{\mu\mu}$ are not applied to increase the number of selected events. The signal samples are scaled as thirty times the normalization obtained with $\sigma(h)$ as predicted in the SM, $\mathcal{B}(h \to aa) = 10\%$, and considering decays of the pseudoscalar a boson to leptons only.

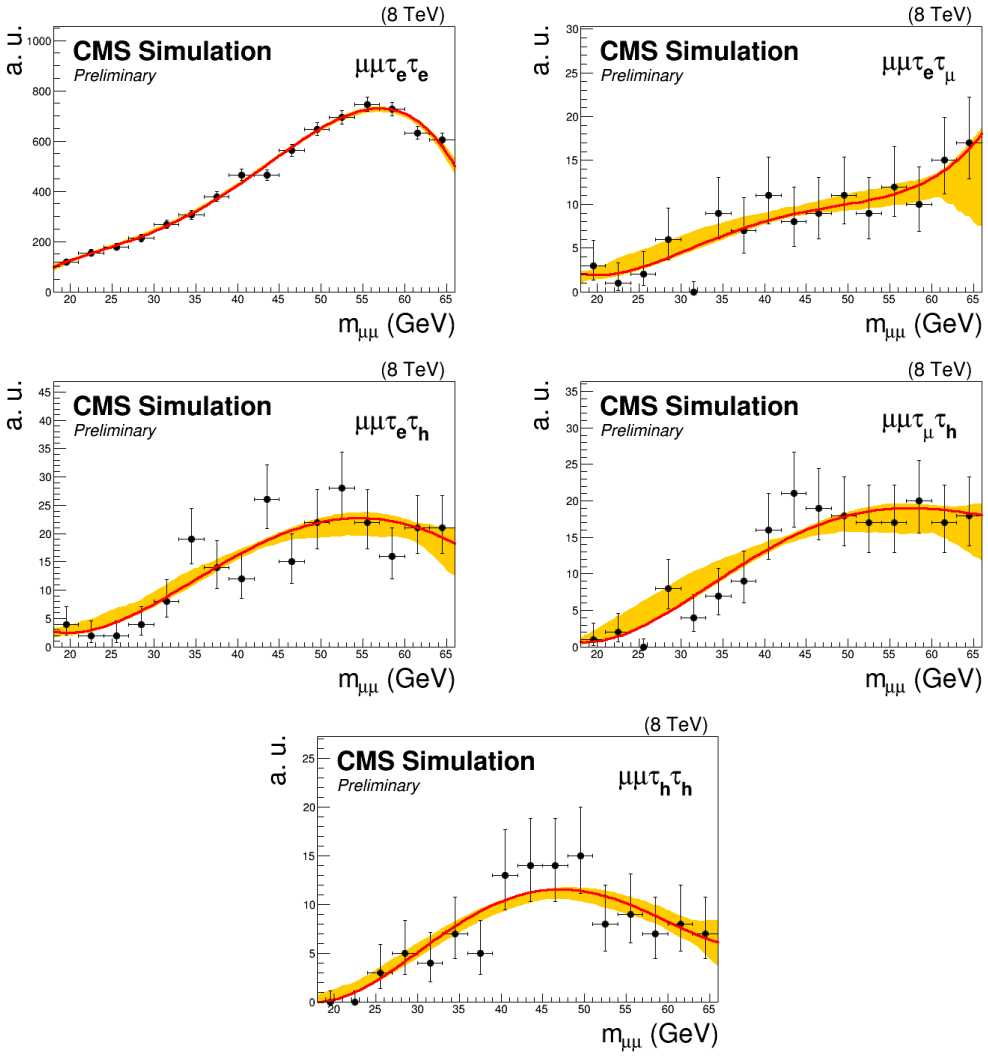

Figure 2: Modeling of the ZZ background, estimated from MC, using fifth-degree Bernstein polynomials, in the $\mu\mu\tau_e\tau_e$ (top left), $\mu\mu\tau_e\tau_\mu$ (top right), $\mu\mu\tau_e\tau_h$ (center left), $\mu\mu\tau_\mu\tau_h$ (center right), and $\mu\mu\tau_h\tau_h$ (bottom) final states. The black dots correspond to events selected in MC.

Except in the $\mu\mu\tau_e\tau_e$ final state, the reducible background dominates by far the ZZ contribution. The reducible background is modeled with a third-degree Bernstein polynomial, chosen to optimize the fit quality and to be positive over the full mass range. The fit uncertainties are taken into account in the limit setting procedure described later. The fits in the different final states are shown in Fig. 3.

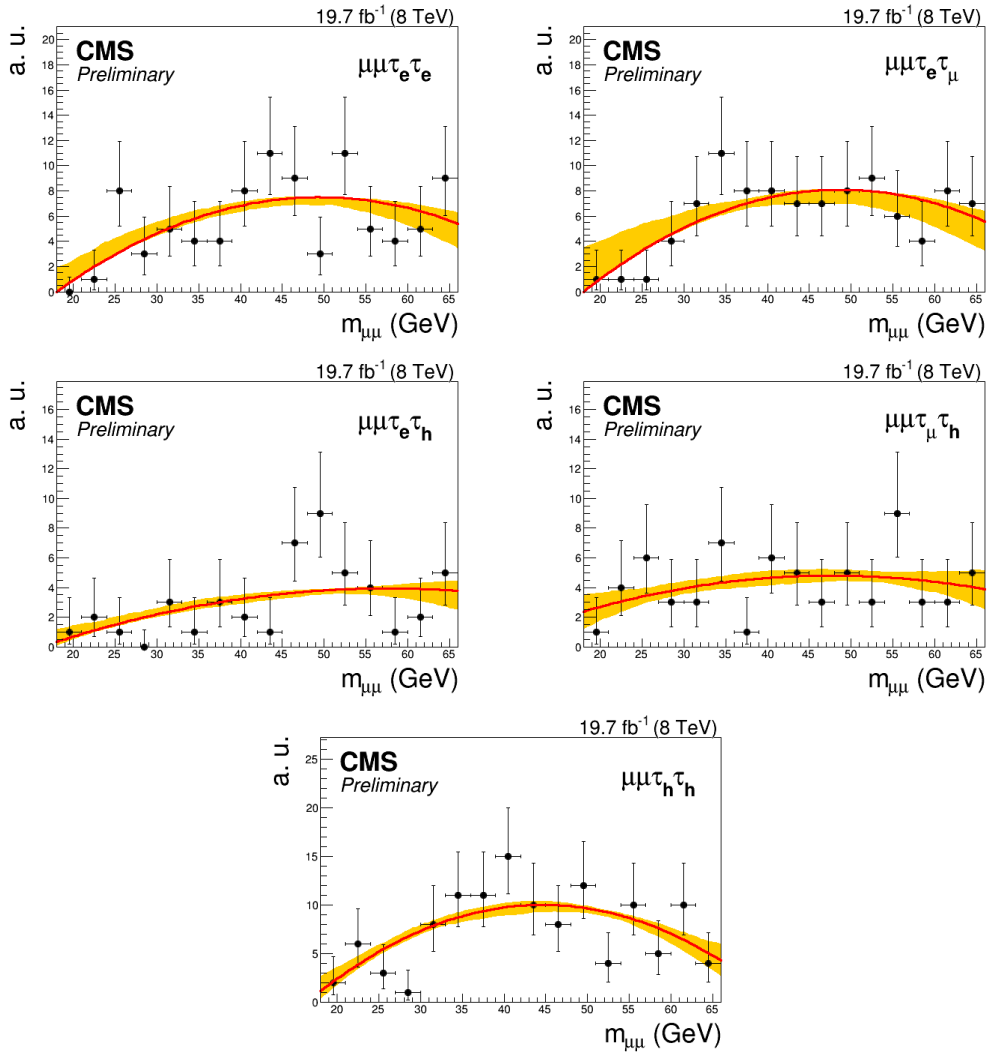

Figure 3: Modeling of the reducible background with third-order Bernstein polynomials, in the $\mu\mu\tau_e\tau_e$ (top left), $\mu\mu\tau_e\tau_\mu$ (top right), $\mu\mu\tau_e\tau_h$ (center left), $\mu\mu\tau_\mu\tau_h$ (center right), and $\mu\mu\tau_h\tau_h$ (bottom) final states. The black dots correspond to observed events selected in control regions, as described in Chapter 4.

6 Systematic uncertainties

Experimental uncertainties include the uncertainties on the lepton identification efficiencies: 6% per hadronic tau, 2% per electron and 1% per muon. In addition, the uncertainty on the measured integrated luminosity amounts to 2.6% in 2012 [27]. The veto on events with b-tagged jets introduces a 1% uncertainty on the yield of processes estimated from MC, whereas 1% uncertainty is considered to account for the trigger efficiency uncertainty. The hadronic tau energy scale is varied by $\pm$ 3% [23], and the change in yield is measured to be between 0 and

10% depending on the final state. This uncertainty does not affect the shape of the $m_{\mu\mu}$ distributions, and is treated as uncorrelated for final states using taus with different isolation working points. The muon energy scale uncertainty, amounting to 0.2%, is found to shift the mean of the signal distributions by up to 0.2%; this is taken into account as a parametric uncertainty on the mean of the signal distributions.

Statistical uncertainties on the parameterization of the signal are accounted for through the uncertainties on the fit parameters describing the signal shape. The shape uncertainties of the reducible background are taken into account with three uncorrelated parameters arising from the fit uncertainties of the third-order Berstein polynomials. The uncertainty on the normalization of the reducible background is obtained from varying the fit functions of the misidentification rates within their uncertainties. Changes in yields lie between 25% and 50%; uncertainties related to a given misidentification rate are correlated between corresponding final states.

Because of the limited number of MC events after the full selection, an uncertainty between 1 and 15% depending on the final state is attributed to the ZZ background. This uncertainty is uncorrelated between all final states. Additionally, theoretical uncertainties are considered for the ZZ background to account for uncertainties in the parton distribution functions (PDF), and for the variations of the renormalization and factorization scales. No shape systematic is considered on the ZZ background; as it is a mostly subdominant background the use of another background model would have an impact on the final exclusion limits less than 1%.

Finally, 10% uncertainty is attributed to the signal prediction to reflect theory uncertainties, including uncertainties on the PDF, and an additional yield uncertainty (between 5 and 8% depending on the final state), related to the efficiency interpolation, is taken into account for signal samples.

All sources of uncertainties are reported in Tab. 2, together with the change on yields or shapes they imply for the different processes.

7 Results

In 2HDM and by extension 2HDM+S, the ratio of the decay widths of a pseudoscalar boson to different types of leptons only depends on the masses of these leptons. In particular in the case of muons and tau leptons, one has:

$$\frac{\Gamma(a \to \mu\mu)}{\Gamma(a \to \tau\tau)} = \frac{m_\mu^2 \sqrt{1 - (2m_\mu/m_a)^2}}{m_\tau^2 \sqrt{1 - (2m_\tau/m_a)^2}}. \tag{2}$$

We use this relation to set upper limits on the production of $h \to aa$ relative to the SM h production (including gluon-gluon fusion, vector boson fusion and associated production with a W boson, a Z boson or a pair of top quarks, with cross sections respectively equal to 19.3, 1.58, 0.70, 0.42 and 0.13 pb), scaled by $\mathcal{B}(a \to \tau\tau)^2$. In the hypothesis where the pseudoscalar a boson only decays to leptons, one has $\mathcal{B}(a \to \tau\tau) > 0.995$ for all a boson masses between 20 and 62.5 GeV. This hypothesis is a good approximation in 2HDM+S type-3 with large values of $\tan\beta$.

The parameterized di-muon mass distributions are shown in Fig. 4 for the five different final states. The signal samples, for a mass $m_a = 40$ GeV, are scaled with $\sigma(h)$ as expected in the SM including all production modes, $\mathcal{B}(h \to aa) = 10\%$ and considering decays of the pseudoscalar a boson to leptons only ($\mathcal{B}(a \to \tau\tau) + \mathcal{B}(a \to \mu\mu) = 1$, where the decay to electrons is neglected).

Table 2: Systematic uncertainties on the yields or shapes of the signal, ZZ and reducible processes. The relative change in yields resulting from a variation of the nuisance parameter equivalent to one standard deviation is indicated.

Systematic uncertainty	Relative change in yield		
	Signal	ZZ	Reducible backgrounds
Luminosity	2.6%	2.6%	-
Trigger	1%	1%	-
Tau identification	0-12%	0-12%	-
b-Jet veto	1%	1%	-
Tau energy scale	0-10%	0-10%	-
Electron identification	0-4%	0-4%	-
Muon identification	2-4%	2-4%	-
Signal prediction	10%	-	-
Signal efficiency	5-8%	-	-
PDF	-	5%	-
QCD scale VV	-	6%	-
ZZ statistics in MC	-	1-15%	-
Reducible background normalization	-	-	25-50%
Reducible background shape	-	-	shape only
Signal modeling	shape only	-	-
Muon energy scale	shape only	-	-

Table 3: Expected and observed yields in the different final states. The signal samples are scaled with $\sigma(h)$ as expected in SM, $\mathcal{B}(h \to aa) = 10\%$ and considering decays of the pseudoscalar a boson to leptons only. The background yields are obtained after a maximum likelihood fit to observed data, taking into account the systematic uncertainties described in Chapter 6.

	Signal		Backgrounds			Obs.
	m_a = 20 GeV	m_a = 60 GeV	ZZ	Reducible	Total	
$\mu\mu\tau_e\tau_e$	0.20±0.02	0.58±0.06	4.64±0.39	2.49±1.03	7.13±1.10	8
$\mu\mu\tau_e\tau_\mu$	0.58±0.08	1.42±0.16	0.10±0.01	1.70±0.74	1.80±0.74	2
$\mu\mu\tau_e\tau_h$	0.74±0.08	2.02±0.20	0.16±0.02	5.65±1.77	5.81±1.77	5
$\mu\mu\tau_\mu\tau_h$	0.96±0.10	2.30±0.22	0.13±0.02	0.99±0.31	1.12±0.31	1
$\mu\mu\tau_h\tau_h$	0.60±0.06	1.90±0.18	0.06±0.01	4.64±0.98	4.70±0.98	3
Combined	3.08±0.31	8.22±0.82	5.09±0.39	15.47±2.41	20.56±2.44	19

The expression 2 is used to express $\mathcal{B}(a \to \mu\mu)$ as a function of $\mathcal{B}(a \to \tau\tau)$. The expected and observed yields are shown in Tab. 3.

An unbinned maximum likelihood fit to data is performed, and upper limits are set at 95% confidence level using the modified frequentist CL_s construction [28, 29], without asymptotic approximation. The procedure takes into account the different yield and shape systematic uncertainties described in the previous chapter. The upper limits set in each final state in the mass range between 20 and 62.5 GeV are shown in Fig. 5, and range from 4 to 15% for the combination. When taking into account the look-elsewhere effect, no excess has a global significance larger than 2 standard deviations.

As the branching fractions of the pseudoscalar boson to SM particles are known when a type of

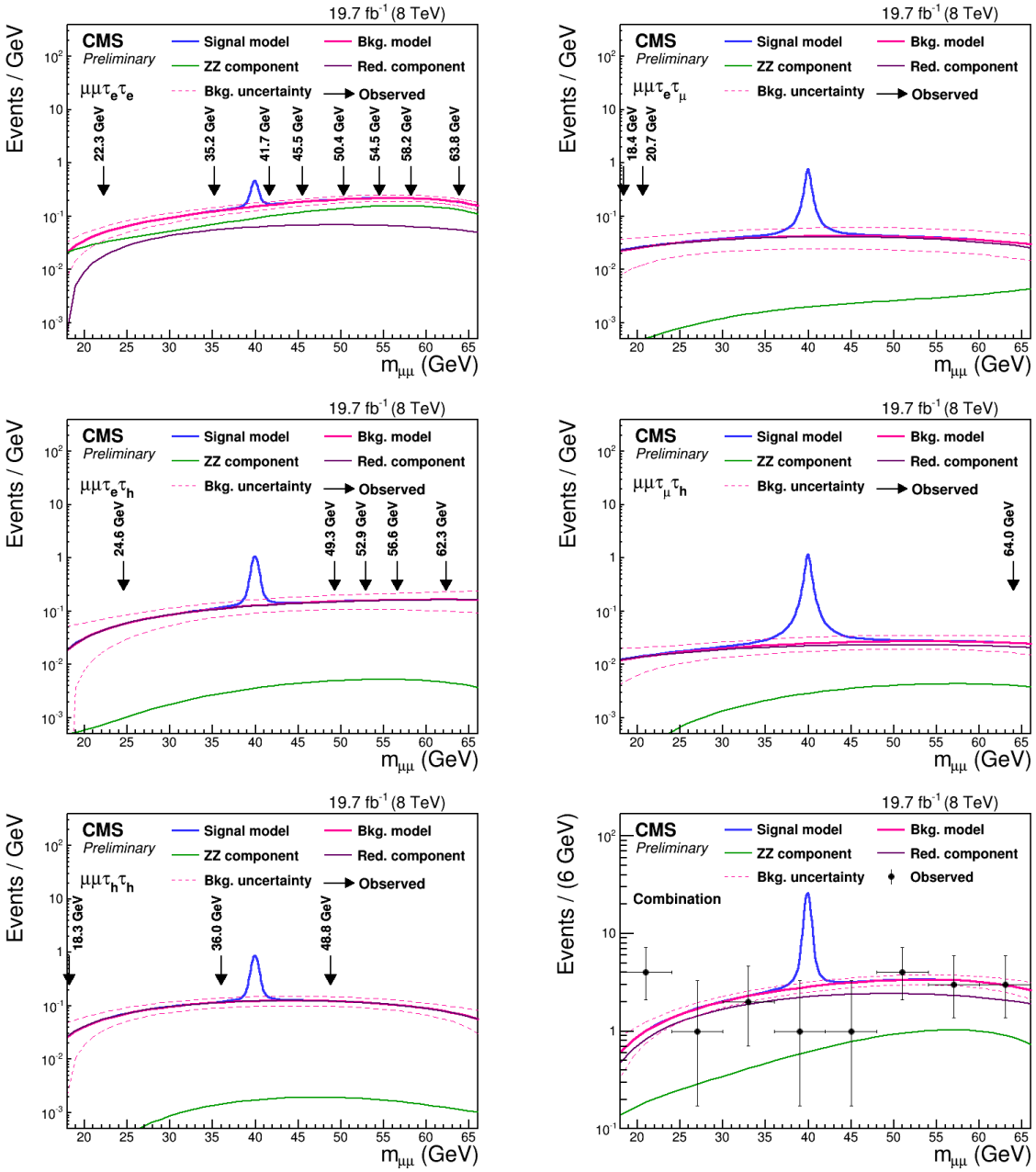

Figure 4: Background and signal ($m_a = 40$ GeV) models, scaled to their expected yields, in the $\mu\mu\tau_e\tau_e$ (top left), $\mu\mu\tau_e\tau_\mu$ (top right), $\mu\mu\tau_e\tau_h$ (center left), $\mu\mu\tau_\mu\tau_h$ (center right), and $\mu\mu\tau_h\tau_h$ (bottom left) final states, and their combination (bottom right). The two components that form the background model, ZZ and reducible processes, are drawn. Every observed event in the individual decay channels is represented by an arrow, together with its measured $m_{\mu\mu}$ value; while in the combined mass plot data are binned in a histogram. The signal samples are scaled with $\sigma(h)$ as predicted in the SM, $\mathcal{B}(h \to aa) = 10\%$ and considering decays of the pseudoscalar a boson to leptons only. The results are shown after a simultaneous maximum likelihood fit that takes into account the systematic uncertainties described in Chapter 6.

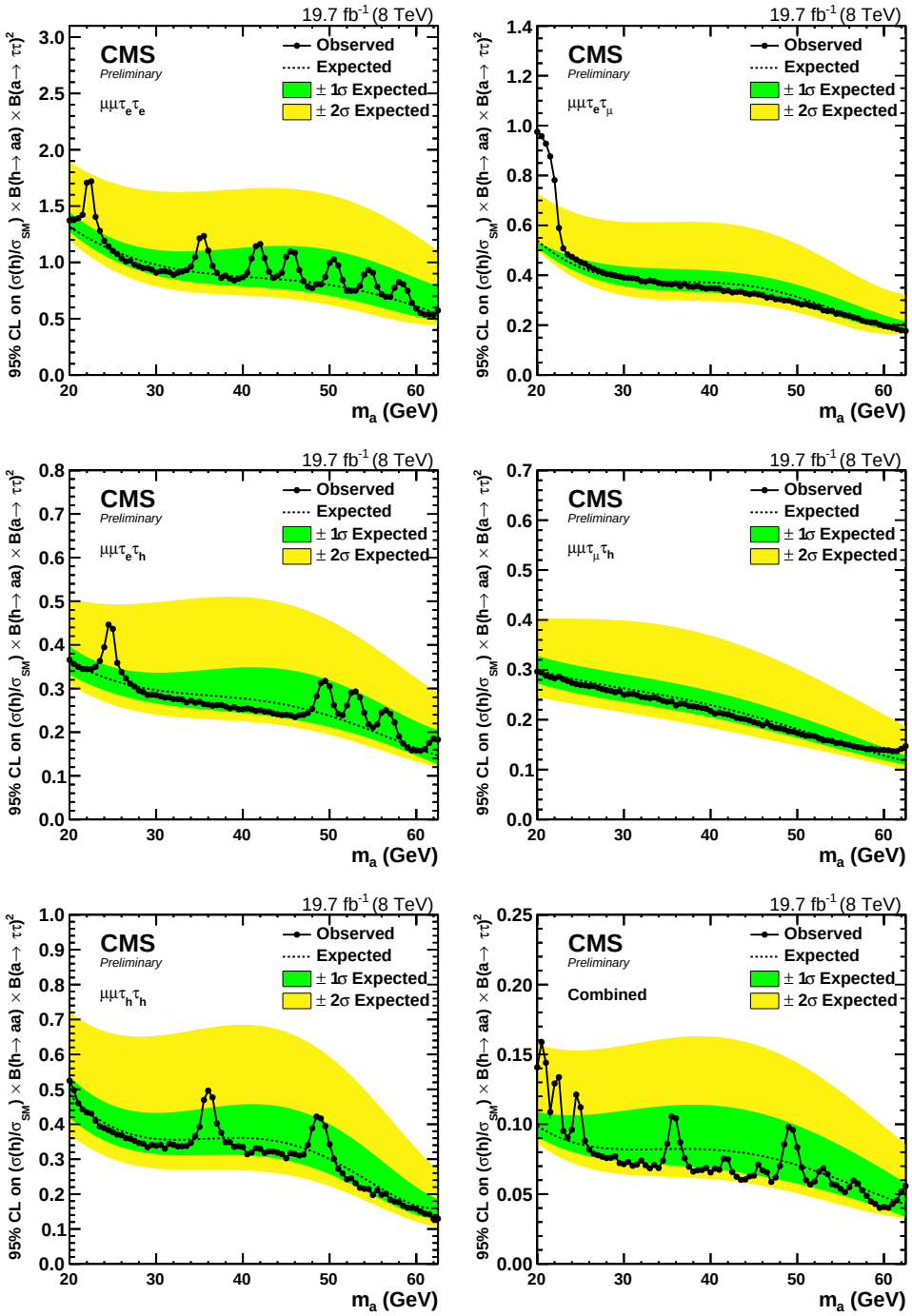

Figure 5: Expected upper limits at 95% CL on the production of $h \to aa$ relative to the SM h production, scaled by $\mathcal{B}(a \to \tau\tau)^2$, in the $\mu\mu\tau_e\tau_e$ (top left), $\mu\mu\tau_e\tau_\mu$ (top right), $\mu\mu\tau_e\tau_h$ (center left), $\mu\mu\tau_\mu\tau_h$ (center right), and $\mu\mu\tau_h\tau_h$ (bottom left) final states, and for the combination of these five final states (bottom right). $\mathcal{B}(a \to \tau\tau)^2$ is close to 1 in the hypothesis where the pseudoscalar a boson does not decay to quarks. No excess has a global significance larger than 2 standard deviations.

2HDM+S and a value of $\tan\beta$ are chosen, the combined results can be interpreted as a limit on $\frac{\sigma(h)}{\sigma_{SM}} \times \mathcal{B}(h \to aa)$ in the $m_a - \tan\beta$ plane for every type of 2HDM+S. The analysis is sensitive to large values of $\tan\beta$ in 2HDM+S type-3, and to small values of $\tan\beta$ in 2HDM+S type-4, as shown in Fig. 6. It is however not sensitive yet to 2HDM+S type-1 and type-2.

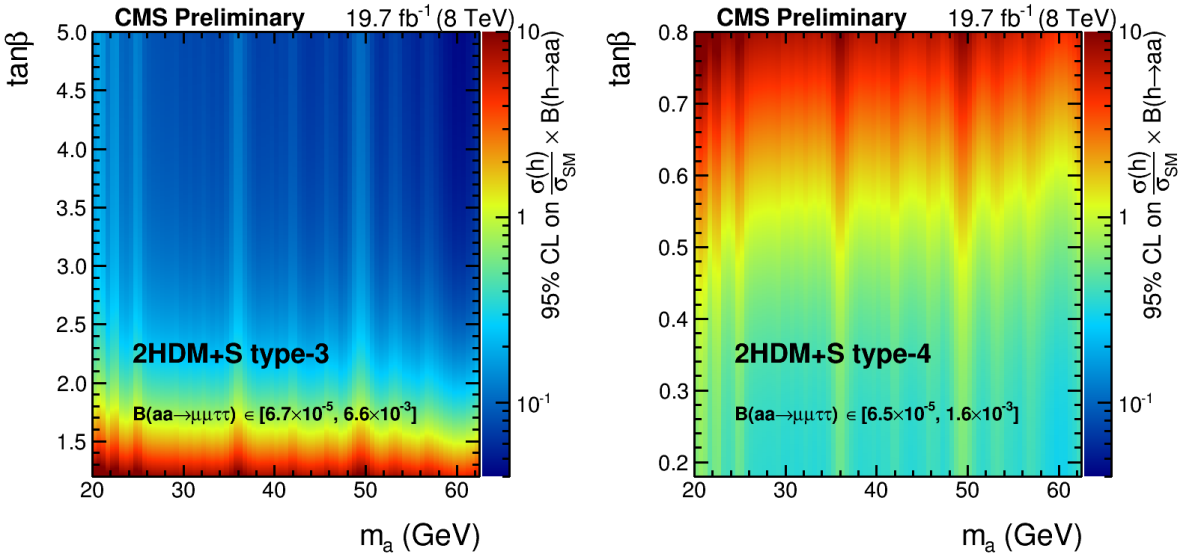

Figure 6: Observed upper limits at 95% CL on $\frac{\sigma(h)}{\sigma_{SM}} \times \mathcal{B}(h \to aa)$ for the combination of all di-tau final states, in 2HDM+S type-3 (left) and type-4 (right). The branching fraction $\mathcal{B}(aa \to \mu\mu\tau\tau)$ ranges between 6.7×10^{-5} and 6.6×10^{-3} in 2HDM+S type-3 for the m_a and $\tan\beta$ values shown in the figure, while it ranges between 6.5×10^{-5} and 1.6×10^{-3} in 2HDM+S type-4 in the right figure. The branching fractions of the pseudoscalar boson to SM particles have been computed following the prescriptions in [7].

8 Comparison with other exotic h decay searches

Three other searches for exotic decays of the h boson to a pair of lighter pseudoscalar bosons have been performed with the data collected by the CMS detector at 8 TeV center-of-mass energy. The $h \to aa \to \mu\mu\mu\mu$ analysis covers pseudoscalar boson masses between 0.25 and 3.55 GeV [10], whereas two $h \to aa \to \tau\tau\tau\tau$ searches cover pseudoscalar masses between 4 and 8 GeV, or 5 and 15 GeV, with different boosted tau reconstruction techniques [11, 12]. None of these analyses has seen any hint of new physics beyond the SM.

Because $\mathcal{B}(a \to \tau\tau)$ is directly proportional to $\mathcal{B}(a \to \mu\mu)$ in any type of 2HDM+S as per equation (2), the results of all analyses can be expressed as exclusion limits on $\frac{\sigma(h)}{\sigma_{SM}} \times \mathcal{B}(h \to aa) \times \mathcal{B}(a \to \mu\mu)^2$, as illustrated in Fig. 7.

In 2HDM+S, the values of the branching fractions of the pseudoscalar boson to SM particles depend on the type of 2HDM+S, on $\tan\beta$, and on the mass of the pseudoscalar boson. They can be computed precisely following the prescriptions in [7] and [30], except for pseudoscalar boson masses between approximatively 3 and 5 GeV, and 9 and 11 GeV, because of decays to quarkonia, and for pseudoscalar boson masses less than 1 GeV because of huge uncertainties in the hadronic region. The largest branching fractions for the $\mu\mu\tau\tau$ final state are obtained in 2HDM+S type-3 at large $\tan\beta$, where the pseudoscalar couplings to leptons are enhanced over

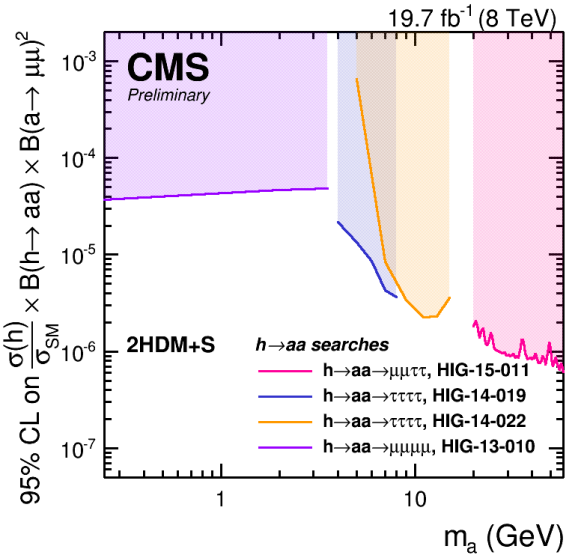

Figure 7: Observed 95% CL exclusion limits on $\frac{\sigma(h)}{\sigma_{SM}} \times \mathcal{B}(h \to aa) \times \mathcal{B}(a \to \mu\mu)^2$ for various exotic h decay searches performed with data collected at 8 TeV with the CMS detector, assuming that the branching fractions of the pseudoscalar boson to muons and to tau leptons follows equation (2).

those to quarks, and in 2HDM+S type-4 at small $\tan\beta$, where the pseudoscalar couplings to leptons and up-type quarks are enhanced over those to down-type quarks. These two scenarios are chosen to compare the reach of all four analyses in terms of limits on $\frac{\sigma(h)}{\sigma_{SM}} \times \mathcal{B}(h \to aa)$, as shown in Fig. 8. The exclusion limit on $\frac{\sigma(h)}{\sigma_{SM}} \times \mathcal{B}(h \to aa) \times \mathcal{B}(a \to \mu\mu)^2$ for the $h \to aa \to \mu\mu\mu\mu$ analysis presented in Fig. 7 is extrapolated from three mass points (0.25, 2.00, 3.55 GeV) to intermediary masses with a third degree polynomial, before being divided by the square of $\mathcal{B}(a \to \mu\mu)$ to obtain limits on $\frac{\sigma(h)}{\sigma_{SM}} \times \mathcal{B}(h \to aa)$. The sudden increase of the exclusion limit for m_a around 2.6 GeV in 2HDM+S type-3 $\tan\beta = 5.0$ is the consequence of the opening of the $a \to cc$ decay channel, whereas the variation of the limit around $m_a = 1.3$ GeV in 2HDM+S type-4 $\tan\beta = 0.5$ is related to an increase of the pseudoscalar boson decay width to gluons because of the change in the number of active flavors in the QCD corrections and in the computation of the running of the strong coupling constant at a renormalization scale equal to m_a.

9 Summary

A search for the exotic decay $h \to aa$ in the final state with two muons and two taus, for pseudoscalar masses between 20 and 62.5 GeV, is performed with data collected by the CMS detector at a center-of-mass energy of 8 TeV in 2012. Such a decay is motivated in models like 2HDM+S. Given the good di-muon mass resolution, limits are obtained from an unbinned fit of $m_{\mu\mu}$ distributions in five final states. Expected upper limits are set on the relative production of $h \to aa$ relatively to the SM h production, scaled by the square of the branching fraction $\mathcal{B}(a \to \tau\tau)$. In the hypothesis where the pseudoscalar a boson does not decay to quarks, which is a good approximation in 2HDM+S type-3 with large $\tan\beta$, $\mathcal{B}(a \to \tau\tau)$ is approximately equal to unity and $\mathcal{B}(h \to aa)$ is measured to be less than a value ranging between 0.04 and 0.15 at 95% CL, depending on the pseudoscalar mass probed. Model-dependent limits are also

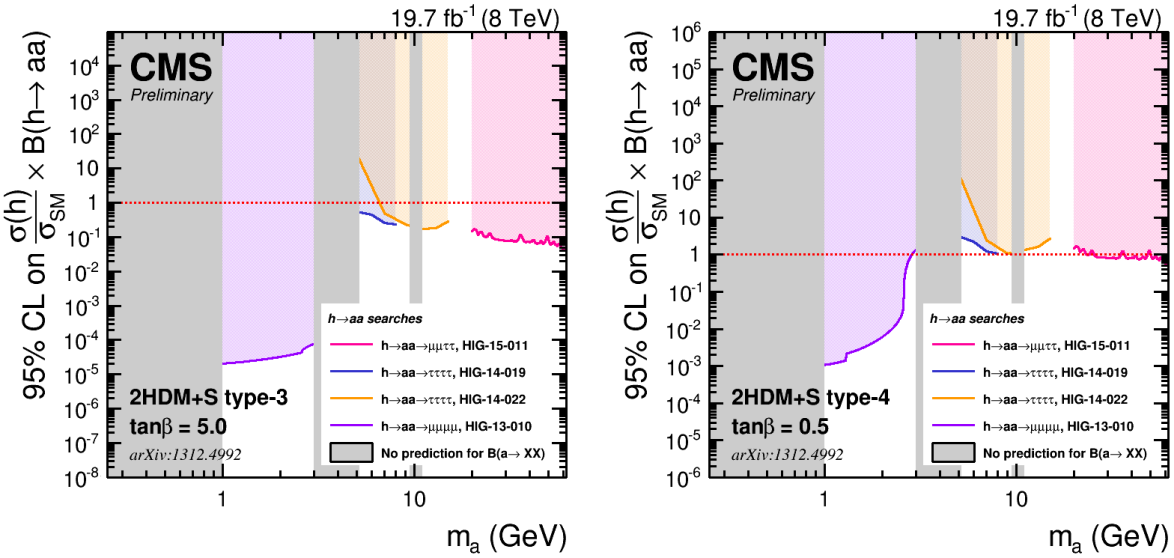

Figure 8: 95% CL on $\sigma(h)/\sigma_{SM} \times \mathcal{B}(h \to aa)$ in 2HDM+S type-3 $\tan\beta = 5$ (left) and type-4 $\tan\beta = 0.5$ (right) for exotic h decay searches performed with data collected at 8 TeV center-of-mass energy. The branching fractions of the pseudoscalar boson to SM particles are computed following the prescriptions in [7].

set on $\frac{\sigma(h)}{\sigma_{SM}} \times \mathcal{B}(h \to aa)$ in the $m_a - \tan\beta$ plane in 2HDM+S type-3 and type-4, and the analysis is compared to other exotic h decay searches performed with 8 TeV data collected by the CMS detector.

References

[1] CMS Collaboration, "Observation of a new boson at a mass of 125 GeV with the CMS experiment at the LHC", *Phys.Lett.* **B716** (2012) 30–61, doi:10.1016/j.physletb.2012.08.021, arXiv:1207.7235.

[2] ATLAS Collaboration, "Observation of a new particle in the search for the Standard Model Higgs boson with the ATLAS detector at the LHC", *Phys.Lett.* **B716** (2012) 1–29, doi:10.1016/j.physletb.2012.08.020, arXiv:1207.7214.

[3] CMS Collaboration, "Precise determination of the mass of the Higgs boson and tests of compatibility of its couplings with the standard model predictions using proton collisions at 7 and 8 TeV", *Eur. Phys. J.* **C75** (2015), no. 5, 212, doi:10.1140/epjc/s10052-015-3351-7, arXiv:1412.8662.

[4] ATLAS Collaboration, "Measurements of the Higgs boson production and decay rates and coupling strengths using pp collision data at $\sqrt{s} = 7$ and 8 TeV in the ATLAS experiment", *Eur. Phys. J.* **C76** (2016), no. 1, 6, doi:10.1140/epjc/s10052-015-3769-y, arXiv:1507.04548.

[5] G. Belanger et al., "Status of invisible Higgs decays", *Phys. Lett. B* **723** (2013) 340, doi:10.1016/j.physletb.2013.05.024, arXiv:1302.5694.

[6] D. Curtin, R. Essig, and Y.-M. Zhong, "Uncovering light scalars with exotic Higgs decays to bb$\mu\mu$", *JHEP* **1506** (2015) 025, doi:10.1007/JHEP06(2015)025, arXiv:1412.4779.

[7] D. Curtin et al., "Exotic decays of the 125 GeV Higgs boson", *Phys. Rev. D* **90** (2014) 075004, doi:10.1103/PhysRevD.90.075004, arXiv:1312.4992.

[8] C. Englert, T. Plehn, D. Zerwas, and P. M. Zerwas, "Exploring the Higgs portal", *Phys. Lett.* **B703** (2011) 298–305, doi:10.1016/j.physletb.2011.08.002, arXiv:1106.3097.

[9] ATLAS Collaboration, "Search for Higgs bosons decaying to *aa* in the $\mu\mu\tau\tau$ final state in pp collisions at $\sqrt{s} = 8$ TeV with the ATLAS experiment", *Phys. Rev.* **D92** (2015), no. 5, 052002, doi:10.1103/PhysRevD.92.052002, arXiv:1505.01609.

[10] CMS Collaboration, "A search for pair production of new light bosons decaying into muons", *Phys. Lett.* **B752** (2016) 146–168, doi:10.1016/j.physletb.2015.10.067, arXiv:1506.00424.

[11] CMS Collaboration, "Search for a very light NMSSM Higgs boson produced in decays of the 125 GeV scalar boson and decaying into tau leptons in pp collisions at sqrt(s) = 8 TeV", *JHEP* **01** (2016) 079, doi:10.1007/JHEP01(2016)079, arXiv:1510.06534.

[12] CMS Collaboration, "Search for Higgs Decays to New Light Bosons in Boosted Tau Final States", CMS Physics Analysis Summary CMS-PAS-HIG-14-022, 2015.

[13] CMS Collaboration, "The CMS experiment at the CERN LHC", *JINST* **3** (2008) S08004, doi:10.1088/1748-0221/3/08/S08004.

[14] J. Alwall et al., "MadGraph/MadEvent v4: the new web generation", *JHEP* **09** (2007) 028, doi:10.1088/1126-6708/2007/09/028, arXiv:hep-ph/0706.2334.

[15] T. Sjöstrand, S. Mrenna, and P. Skands, "PYTHIA 6.4 physics and manual", *JHEP* **05** (2006) 026, doi:10.1088/1126-6708/2006/05/026, arXiv:hep-ph/0603175.

[16] S. Jadach, Z. Was, R. Decker, and J. H. Kuhn, "The Tau Decay Library Tauola: Version 2.4", *Comput. Phys. Commun.* **76** (1993) 361.

[17] S. Agostinelli et al., "G4–a simulation toolkit", *Nuclear Instruments and Methods in Physics Research Section A: Accelerators, Spectrometers, Detectors and Associated Equipment* **506** (2003), no. 3, 250 – 303, doi:10.1016/S0168-9002(03)01368-8.

[18] CMS Collaboration, "Particle-Flow Event Reconstruction in CMS and Performance for Jets, Taus, and MET", CMS Physics Analysis Summary CMS-PAS-PFT-09-001, 2009.

[19] CMS Collaboration, "Commissioning of the Particle-flow Event Reconstruction with the first LHC collisions recorded in the CMS detector", CMS Physics Analysis Summary CMS-PAS-PFT-10-001, 2010.

[20] CMS Collaboration, "Performance of CMS muon reconstruction in pp collision events at $\sqrt{s} = 7$ TeV", *JINST* **7** (2012) P10002, doi:10.1088/1748-0221/7/10/P10002, arXiv:1206.4071.

[21] CMS Collaboration, "Performance of electron reconstruction and selection with the CMS detector in proton-proton collisions at $\sqrt{s}$= 8 TeV", *JINST* **10** (2015), no. 6, P06005, doi:10.1088/1748-0221/10/06/P06005, arXiv:1502.02701.

[22] CMS Collaboration, "Performance of tau-lepton reconstruction and identification in CMS", *JINST* **7** (2012) P01001, doi:10.1088/1748-0221/7/01/P01001, arXiv:1109.6034.

[23] CMS Collaboration, "Reconstruction and identification of τ lepton decays to hadrons and ν_τ at CMS", *JINST* **11** (2016), no. 01, P01019, doi:10.1088/1748-0221/11/01/P01019, arXiv:1510.07488.

[24] CMS Collaboration, "Identification of b-quark jets with the CMS experiment", *JINST* **8** (2013) P04013, doi:10.1088/1748-0221/8/04/P04013, arXiv:1211.4462.

[25] L. Bianchini, J. Conway, E. K. Friis, and C. Veelken, "Reconstruction of the Higgs mass in $H \to \tau\tau$ Events by Dynamical Likelihood techniques", *J.Phys.Conf.Ser.* **513** (2014) 022035, doi:10.1088/1742-6596/513/2/022035.

[26] J. M. Campbell, R. K. Ellis, and C. Williams, "Vector boson pair production at the LHC", *JHEP* **1107** (2011) 018, doi:10.1007/JHEP07(2011)018, arXiv:1105.0020.

[27] CMS Collaboration, "CMS Luminosity Based on Pixel Cluster Counting - Summer 2013 Update", CMS Physics Analysis Summary CMS-PAS-LUM-13-001, 2013.

[28] A. L. Read, "Modified frequentist analysis of search results (the CLs method)", CERN Report CERN-OPEN-2000-005, 2000.

[29] T. Junk, "Confidence level computation for combining searches with small statistics", *Nucl. Instrum. Meth.* **A434** (1999) 435–443, doi:10.1016/S0168-9002(99)00498-2, arXiv:hep-ex/9902006.

[30] A. Djouadi, "The Anatomy of electro-weak symmetry breaking. I: The Higgs boson in the standard model", *Phys. Rept.* **457** (2008) 1–216, doi:10.1016/j.physrep.2007.10.004, arXiv:hep-ph/0503172.